PAPER

Check for updates

Structures and electric properties of PANI/polymorphic-ZrO$_2$ composites

Munaji,[*ab] Mochamad Zainuri[a] and Triwikantoro [*a]

A polyaniline/zirconia (PANI/ZrO$_2$) composite has been successfully synthesized using an *in situ* method with HCl used as a doping agent, SDBS as a surfactant and APS as an oxidant. The filler variations were comprised of various phases, which are amorphous, tetragonal, monoclinic and a mixture of tetragonal–monoclinic and varied volumes of 0, 2.5, 5.0, 7.5 and 10%. Amorphous, tetragonal and a mixture of tetragonal–monoclinic ZrO$_2$ were obtained from purifying natural zircon sand (ZrSiO$_4$), while monoclinic ZrO$_2$ was obtained from commercial materials. The structure characterisation was performed using X-ray diffraction and Fourier Transform Infrared (FTIR). The morphology was observed using a Scanning Electron Microscope (SEM). The electrical properties of impedance, dielectric constant and dielectric losses, and electrical conductivity were characterised using Electrochemical Impedance Spectroscopy (EIS). The research results showed that the filler phase had an effect towards the electrical properties of PANI/ZrO$_2$. The impedance of PANI as well as PANI/ZrO$_2$ showed a constant phase element (CPE) behaviour with impedance values of 9.87, 9.16, 13.31, and 79.59 kΩ for the composites with amorphous filler, monoclinic filler, tetragonal filler, and tetragonal–monoclinic filler, respectively. The dielectric constant and dielectric losses decreased with the increasing amount of ZrO$_2$ filler. The AC conductivity of PANI/ZrO$_2$ was found to be lower when compared to PANI for all of the filler phases and volume fractions.

1. Introduction

Zirconium oxide (ZrO$_2$), or more widely known as zirconia, is a ceramic material with excellent heat resistance due to its high melting point. This material has three polymorphism phase possibilities, which are tetragonal, monoclinic, and cubic.[1] ZrO$_2$ can be synthesized from zircon (ZrSiO$_4$) using the alkali fusion method. Zircon is obtained from purifying zircon sand and extracted into ZrO$_2$ (amorphous, tetragonal, monoclinic) and other products such as SiO$_2$.[2] The extracted ZrO$_2$ has been further researched by combining it with Al$_2$O$_3$ to produce fake teeth.[3] Other research studies have reported the use of zirconia as an anti-corrosion coating material.[4,5] Besides being combined with another ceramic material, ZrO$_2$ has also been extensively studied as a filler for polymer matrix composites, such as PPy/ZrO$_2$,[6] PMMA/ZrO$_2$,[7,8] PVDF/ZrO$_2$,[9] and PANI/ZrO$_2$.[10–12]

Polyaniline (PANI) is a conductive polymer that has been widely researched as an individual or being combined with other materials. Polyaniline is relatively easy to fabricate, one of which is by using the *in situ* polymerisation.[13,14] The ease in fabricating polyaniline allows it to be combined with other materials, such as metal oxide, commonly referred to as a PANI/

metal oxide composite. PANI/metal oxide composites provide a combination of various material properties. Some PANI/metal oxide composites, for example, PANI/V$_2$O$_5$, are used for energy storage[15] and high energy density supercapacitors.[16] The combination of PANI and WO$_3$ to form a PANI-WO$_3$ composite can be used for gas sensors.[17] In addition, the PANI/TiO$_2$ composite has a photocatalytic activity that can be used as a water-splitting photoanode.[18] PANI-Co$_3$O$_4$ composites are reported to have potential applications as LPG gas sensors at room temperature.[19] Concerning electrical conductivity, the presence of Mn$_3$O$_4$ as a filler in the PANI-Mn$_3$O$_4$ composite gives an increase of up to 1000 times greater than PANI.[20]

In addition to the several benefits of using PANI composites described above, polyaniline has been further studied as an anticorrosive coating material, where the anticorrosive properties are affected by the preparation method.[21] In several explorations of anticorrosive properties, a combination of polyaniline with metal oxides such as PANI/SiO$_2$,[22] PANI/TiO$_2$,[23] and PANI/ZrO$_2$ (ref. 24) have been studied. The anticorrosive behavior of PANI/ZrO$_2$ is related to the electrical properties. Thus, a comprehensive initial study is needed regarding the electrical properties of PANI/ZrO$_2$. Researches on PANI/ZrO$_2$ could be reviewed from different standpoints in terms of the filling materials used for ZrO$_2$, whereby among them are the material source, synthesis methods, particle sizes, and structures/phases. A study on the synthesis and characterisation of PANI/ZrO$_2$ composite generally use commercial ZrO$_2$ as a filler.[10,24–26]

aDepartment of Physics, Faculty of Science and Data Analytics, Institut Teknologi Sepuluh Nopermber, Kampus ITS Sukolilo, Surabaya, 60111, Indonesia. E-mail: triwi@physics.its.ac.id

bDepartment of Mechanical Engineering, Faculty of Engineering, Universitas Muhammadiyah Ponorogo, Jl. Budi Utomo 10, Ponorogo, 63471, Indonesia

Other researches have specifically reported on ZrO_2 phase being used as filler of PANI/ZrO_2 composite, which are monoclinic[25,27] and tetragonal.[10] Some literature specifically reported on the types of phases being used. In this paper, the synthesis and characterisation of PANI/ZrO_2 composite with ZrO_2 being synthesized from natural zircon sand is reported,[2,3] whereby the zircon sand takes the form of four phase polymorphism, which are amorphous, tetragonal, monoclinic, and a mixture of tetragonal–monoclinic. This becomes an interesting topic to be discussed in order to find out whether there is a characteristic difference of PANI/ZrO_2 composite with ZrO_2 synthesized from natural zircon sand if the filler phases are different. This paper explores the relations between the filler phases with the electrical properties of the composite, which includes impedance, dielectric permittivity and AC conductivity.

2. Experimental

2.1 Materials

Aniline and ammonium peroxodisulfate (APS) were both obtained from Merck, Germany. HCl, NH_4OH, and NaOH were purchased from SAP Chemical, Indonesia. While Sodium dodecylbenzene sulphonate (SDBS) was acquired from HiMedia Laboratories, India. Amorphous, tetragonal, and tetragonal–monoclinic phases ZrO_2 amorphous powder were acquired from zircon sand extraction using the alkali fusion method as outlined in the previous research,[2] while monoclinic ZrO_2 was gained from commercial materials.

2.2 Synthesis of PANI/ZrO_2 composite

PANI/ZrO_2 composite was synthesized using the *in situ* polymerisation method. The first step was making a solution A with the following procedure: 4 ml of aniline was added into 100 ml of HCl 0.9 M before going through a procedure of ultrasonication for 1 hour. Next, zirconia powder was added and ultrasonicated again for 1 hour. On the other hand, 3.05 grams of SDBS was dissolved into 50 ml of water distillation and dripped bit by bit into aniline/HCl/ZrO_2 while being stirred at 500 rpm. Solution B was made by adding 8 grams of APS into 5 ml of distilled water and stirred until a clear colour was obtained.

Next, solution A was placed in an ice pool at 0–6 °C and titrated with solution B while being stirred at 500 rpm. The process of titration was carried out until there was no more solution B left and solution A changed colour to blue. After carrying out the process of titration, the solution was kept being stirred for 3 hours. Subsequently, an adequate amount of methanol was added to emulsify the solution before being washed three times with distilled water and then filtered. The results were dried at 60 °C until a green colour was obtained. As a comparison, PANI was also synthesized with the same procedure, with the only difference being ZrO_2 was used to produce solution A.

2.3 Characterisation

X-Ray diffraction (Philips X'PERT MPD) was used to identify the phases in ZrO_2, PANI, and PANI/ZrO_2. SEM-EDX (Hitachi Flexsem 1000) was used to observe the microstructures. The electrical properties were studied using Electrochemical Impedance Spectroscopy (EIS) Gamry Reference 600. To measure the impedance, the PANI and PANI/ZrO_2 powders were turned into pellets with a diameter of 13 mm and a thickness of 4 mm.

3. Results and discussion

3.1 XRD studies

The X-ray diffraction patterns of ZrO_2, PANI, and PANI/ZrO_2 are shown in Fig. 1(a)–(d). The prefixes a-, t-, and m-in front of the chemical formula ZrO_2 indicate amorphous, tetragonal and monoclinic phases, respectively. Meanwhile, the tm-prefix indicates that the sample contains two phases, tetragonal and monoclinic. The elements within amorphous zirconia are listed in Table 1. Amorphous ZrO_2 was obtained by extracting $ZrSiO_4$ using the alkali fusion method. From Table 1, it is seen that Zr comprises of the majority of elements. Other elements that were also detected include Hf, Si and Ti, however these elements were found at rather low percentages (approximately only at 2%). The Zr percentage obtained was higher compared to the other researches.[2,3] The analysis results using Rietica for ZrO_2 are displayed in Table 2. Three phases were found within the tm-ZrO_2 sample, which are monoclinic (PDF No. 00-083-0940), tetragonal (PDF No. 00-079-1764) and tetragonal $ZrSiO_4$ (PDF No. 00-083-1375).

3.2 FTIR analysis

The FTIR spectrum of ZrO_2, PANI and PANI/ZrO_2 are all shown in Fig. 2. The functional group analysis that matches with the spectrum peaks are listed in Tables 3 and 4. From both of these tables, the peaks of ZrO_2, PANI, and PANI/ZrO_2 all can be obtained. Some of the peaks experienced a shift. These occurred to the peak at 665.46 cm^{-1} for PANI which shifted to 663.53 cm^{-1} for PANI/a-ZrO_2, and likewise the peak for PANI/t-ZrO_2 shifted to 667.39 cm^{-1} for PANI/tm-ZrO_2. Both of these indicate that there were interactions between PANI with ZrO_2.

3.3 Morphology

The morphology of PANI and PANI/ZrO_2 were observed using SEM. Fig. 3 displays the SEM images of PANI and PANI/ZrO_2 being magnified at 1000 times at the top and 5000 times at the bottom. Based on the SEM images, it is seen that PANI morphology forms an irregular shape. The establishment of PANI morphology depends on the synthesis method and the properties of the oxidant used.[13] PANI in this research was synthesized using the *in situ* polymerisation method by using SDBS as a surfactant and HCl as oxidant. The morphology was in the shape of irregular structure, which was dissimilar to the results obtained by Anwer *et al.*[26] where they also synthesized PANI by using *in situ* method with SSA surfactant.

The morphology of the PANI/ZrO_2 did not differ significantly with PANI, where the only difference being the semi-tubular structure formed was bigger. This indicates that PANI has covered the ZrO_2 particles.
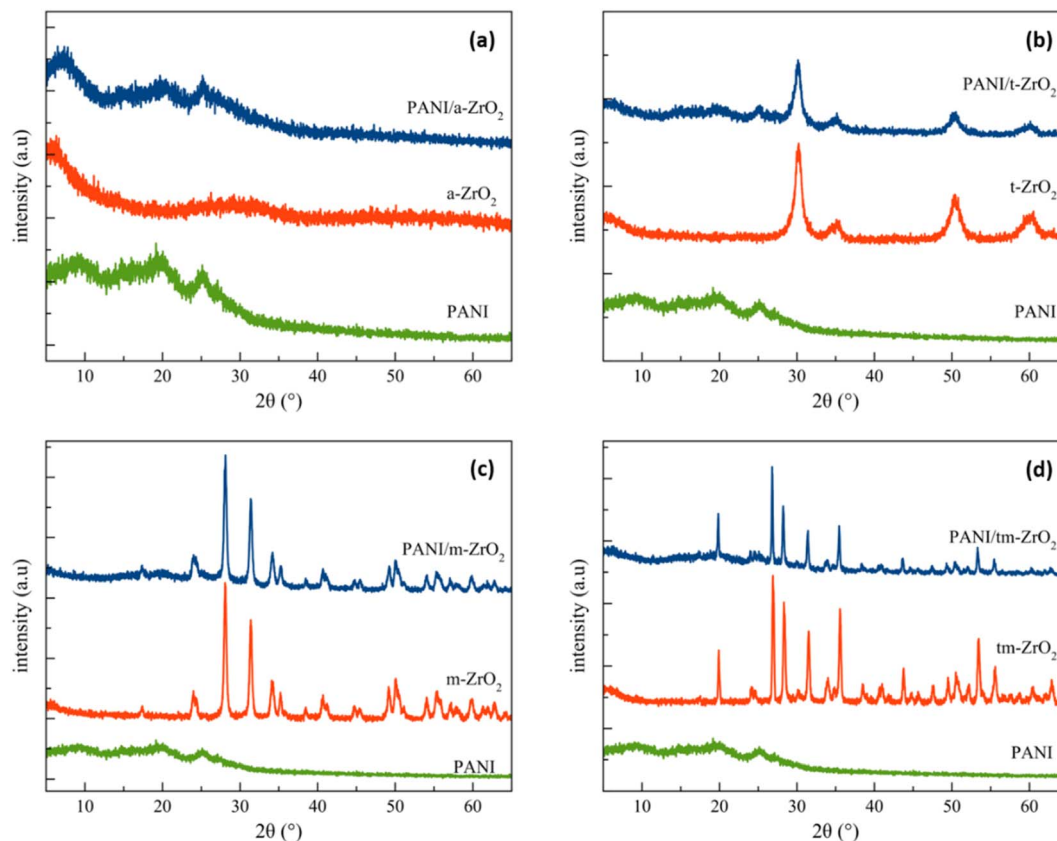
Fig. 1 X-ray diffraction pattern of PANI, ZrO_2 and PANI/ZrO_2. Prefixs a, t, m and tm refers to amorphous, tetragonal, monoclinic and tetragonal–monoclinic, respectively.

Table 1 The elements within a-ZrO_2

Elements	wt%	Elements	wt%
Zr	93.18	Y	0.21
Hf	2.57	Fe	0.15
Si	2.20	Al	0.09
Ti	1.23	Bi	0.05
Ca	0.26	V	0.04

3.4 Impedance analysis

The bulk sample impedances were obtained from Electrochemical Impedance Spectroscopy (EIS) measurements. The impedance graphs of the complexes (real *vs.* imaginary impedance) or the Nyquist plots are displayed in Fig. 4. Fig. 4 exhibits

that the composite with amorphous, tetragonal, and monoclinic ZrO_2 filler have higher impedance compared to PANI. While the composite with multiphase filler (ZrO_2, tetragonal, monoclinic, zircon) has much higher impedance compared to the other four samples.

The effects of filler volume fractions towards the impedance are clearly noticed in Fig. 4b. The impedance value of the composite with 2.5% volume of ZrO_2 is similar to that of PANI. There are also composites with 5.0% and 7.5% filler whose impedance values are similar to each other, although these values are larger compared to PANI and PANI/ZrO_2 with 2.5% volume. The addition of filler volume fractions up to 10% shows a much increase in impedance compared to the other samples.

3.4.1 Equivalent circuit analysis. The impedance curves of the complexes (Nyquist plot) exhibited in Fig. 4 show the curves

Table 2 X-ray diffraction data analysis

Sample	Phases	wt%	Cell parameter (Å)			Refinement parameter	
			a	*b*	*c*	*R*-Bragg	GoF
t-ZrO_2	Tetragonal	100	3.61	3.61	5.22	0.92	2.07
m-ZrO_2	Monoclinic	100	5.14	5.21	5.31	4.20	1.62
	Tetragonal-ZrO_2	9.67	3.59	3.59	5.14	1.19	1.53
tm-ZrO_2-$ZrSiO_4$	Monoclinic-ZrO_2	45.52	5.13	5.14	5.33	1.43	1.53
	Tetragonal-$ZrSiO_4$	44.81	6.61	6.61	5.99	5.01	1.53
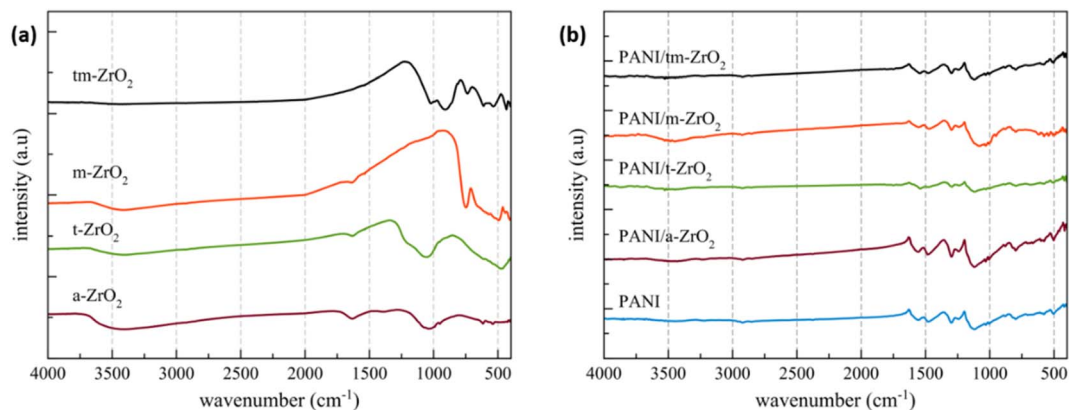
Fig. 2 FTIR spectrum of (a) ZrO_2, (b) PANI and PANI/ZrO_2.

Table 3 Functional groups of ZrO_2

Functionality [Reference]	Wavenumber (cm^{-1})			
	a-ZrO_2	t-ZrO_2	m-ZrO_2	tm-ZrO_2
Zr–O bending vibration[33]	426.28; 484.15	472.58	443.64; 491.86	434.00
Zr–O–Zr bond[34]	952.87; 1041.60	954.80; 1051.24	—	910.43; 1022.31
–(OHO)– and –(HOH)–[6]	1386.86; 1629.90	1635.69	1637.62	—
OH stretching[6]	3408.33	3392.90	3456.55	3421.83

in the shape of depressed semicircle. This type of curve cannot be fitted with the regular electrical circuit models (using resistor and capacitor); however the capacitor element could be exchanged with what is known as Constant Phase Element (CPE).[28] The fitting impedance curves are presented in Fig. 5 and 6. Fitting was conducted by using EchemAnalyst software with equivalent electrical circuit of a parallel R-CPE. The parameter of the fitting results is listed in Table 5.

The CPE impedance can be calculated from eqn (1) as follows.

$$Z_{CPE} = \frac{1}{Q(j\omega)^{\alpha}} \tag{1}$$

In eqn (1), ω denotes the angular frequency and j denotes an imaginary number ($j = \sqrt{-1}$). Whereas α denotes a dimensionless number which is also known as a power number of CPE whose value is between 0 and 1 ($0 < \alpha < 1$). The Q parameter refers to the magnitude of CPE and has a unit of $(Fs^{\alpha-1})$.[29] The value of α in PANI, PANI/a-ZrO_2, PANI/t-ZrO_2 and PANI/m-ZrO_2 are approximately 0.80, whereas in PANI/tm-ZrO_2, it is 0.77. The CPE characteristic points out the unideal behaviour of the

Table 4 Functional groups of PANI and PANI/ZrO_2

| Functionality [Reference]	Wavenumber (cm^{-1})				
	PANI	PANI/a-ZrO_2	PANI/t-ZrO_2	PANI/m-ZrO_2	PANI/tm-ZrO_2
Zr–O bending vibration[33]	—	418.57; 457.14	420.50; 459.07; 472.58	422.42; 445.57; 468.72	418.57; 445.57; 457.14; 472.58
Zr–O–Zr bond[34]	—	1031.95	1030.02	1031.95	1030.02
C–S stretching of benzenoid ring[11]	665.46	663.53	682.82		667.39
Plane bending vibration of C–H[11]	798.56	798.56	796.63	798.56	798.56
Absorption peak of N=Q=N[13]	1120.68	1120.68	1120.68	—	1120.68
Stretching of C–N[11,12]	1244.13; 1298.14	1242.20; 1296.21	1240.27; 1294.28	1240.27; 1298.14	1242.20; 1298.14
Stretching of quinoid ring[11–13]	1477.52	1479.45	1483.31	1469.81	1481.38
C=C ring-stretching vibration of benzenoid form[11–13]	1523.82; 1550.82	1554.68	1539.25	1554.68	1545.03
Plan deformation of –CH methylene group[11]	2922.25	2920.32	2924.18	2926.11	2922.25
OH stretching[6,35]	3408.83	3448.84	—	3446.91	3506.70
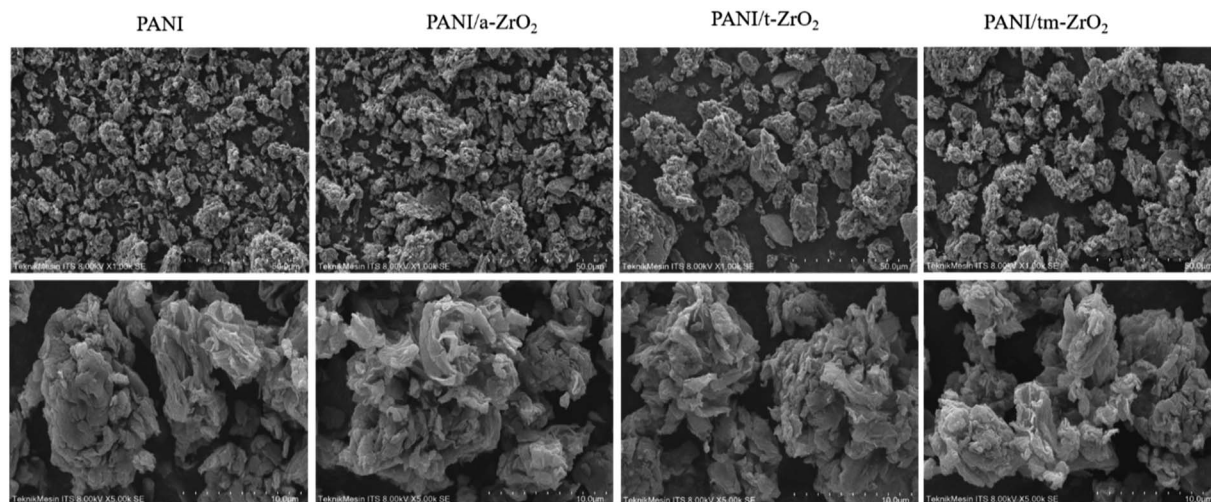
Fig. 3 SEM images of PANI and PANI/ZrO$_2$.

parallel plates capacitor or more widely known as capacitance frequency dispersion due to its dependency towards frequency. This behaviour appears as an effect of the varied current density and potential that passes through the electrode surface. The varied current density can be associated with the inhomogeneity of the electrode surface although not on the macroscopic level, for example, when being related to the surface roughness.[30] The inhomogeneity is more related at the microscopic level, for example, being related to the crystal surface orientation on the surface of the electrodes and the inhomogeneity on the overall surface and the normal direction surface.[31] The phenomenon of CPE on PANI dan PANI/ZrO$_2$ can be related to the SEM data shown in Fig. 3 which shows the morphology in the irregular shapes.

3.4.2 Dielectric constant and dielectric loss. The dielectric constant ε′ and the dielectric losses ε″ are both obtained from eqn (2) and (3), respectively.[32]

$$\varepsilon' = \frac{Z_i}{\omega C_0 \left(Z_r^2 + Z_i^2\right)} \quad (2)$$

$$\varepsilon'' = \frac{Z_r}{\omega C_0 \left(Z_r^2 + Z_i^2\right)} \quad (3)$$

Z_r and Z_i denotes the real and imaginary numbers, respectively, from the impedance complex, whereas ω is the angular frequency.

There is also C_0 which denotes vacuum, which is obtained from eqn (4) as shown.

$$C_0 = \frac{A\varepsilon_0}{d} \quad (4)$$

where ε0 denotes the vacuum permittivity (8.85×10^{-12} F m^{-1}), A denotes the electrode surface area and d denotes the electrode thickness.

The dielectric constant curve depends on the frequency exhibited in Fig. 7. The dielectric constant values, both for PANI and its composites, lie in the range of >1000, and thus making it able to be categorised as a material with a high permittivity (high-k).[36,37] The dielectric constants decrease with the increase
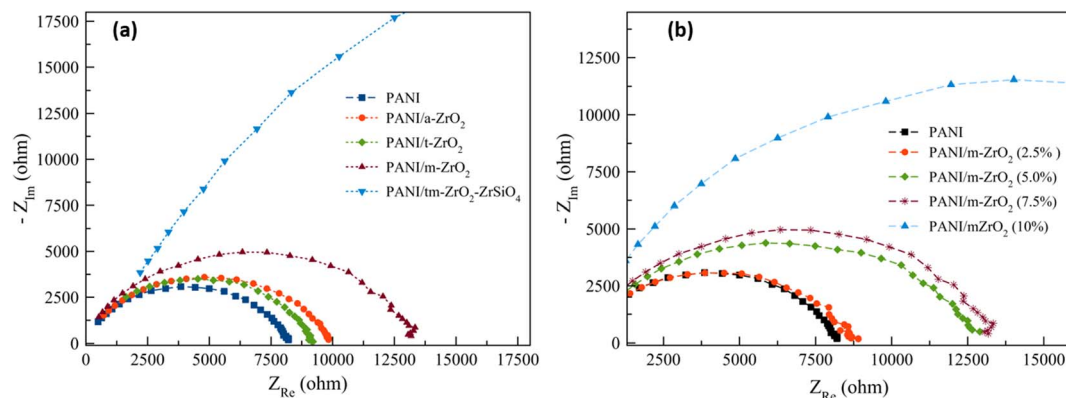

Fig. 4 Impedance of PANI and PANI/ZrO$_2$ complexes: (a) varied filler phase and (b) varied filler volume fractions.

of frequency for all the samples, including PANI and PANI/ZrO_2. The effects of filler phase type towards the composite dielectric constant can be observed from Fig. 7a. All of the PANI/ZrO_2 composites have dielectric constants of less than PANI. Out of all the PANI/ZrO_2 composites, the material with monoclinic ZrO_2 filler has the highest dielectric constant, whereas the material with a mixed filler of ZrO_2–$ZrSiO_4$ has the lowest dielectric constant. The effects of ZrO_2 towards the dielectric constants of the composite materials can be viewed in Fig. 7b. The presence of ZrO_2 decreases the dielectric constant of PANI. The composite with the filler of 2.5% up to 7.5% vol has similar

dielectric constants, whereas at 10% vol has the lowest dielectric constants. The decrease in dielectric constants can be related to the relatively slow relaxation mechanism when compared to the resonant electronic transition or molecular vibrations. On this account, the polaron pinning at small distances through polymer chains would be very easy to carry out and would result in an increase in conductivity by increasing the frequency.[38]

The dielectric losses depending on the frequency are all exhibited in Fig. 8. The dielectric losses also decreased with the increase in frequency. As with the dielectric constants, the
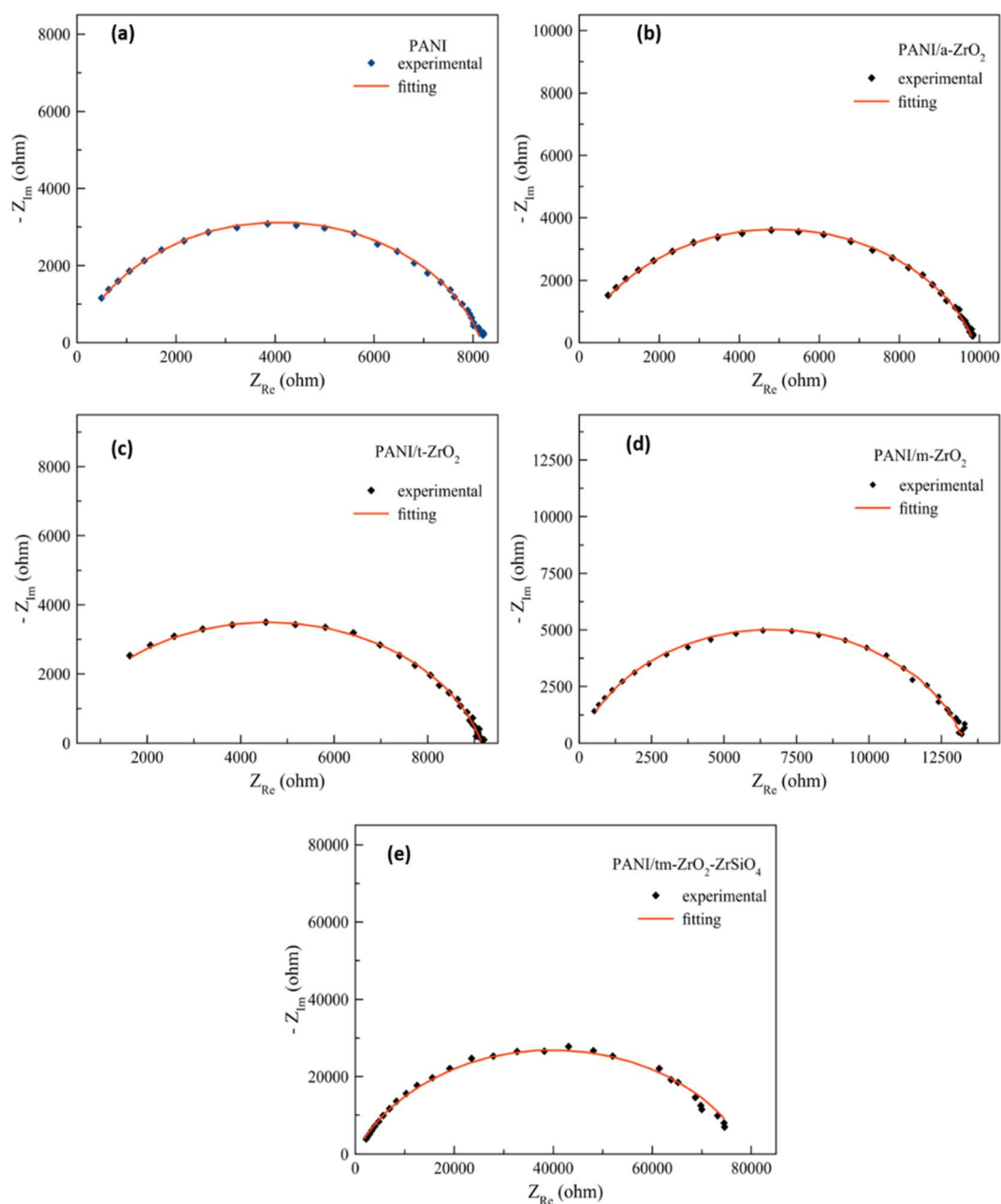

Fig. 5 The results of fitting towards the impedance curve of the complexes: (a) PANI, (b) PANI/a-ZrO_2, (c) PANI/t-ZrO_2, (d) PANI/m-ZrO_2, and (e) PANI/ZrO_2–$ZrSiO_4$.
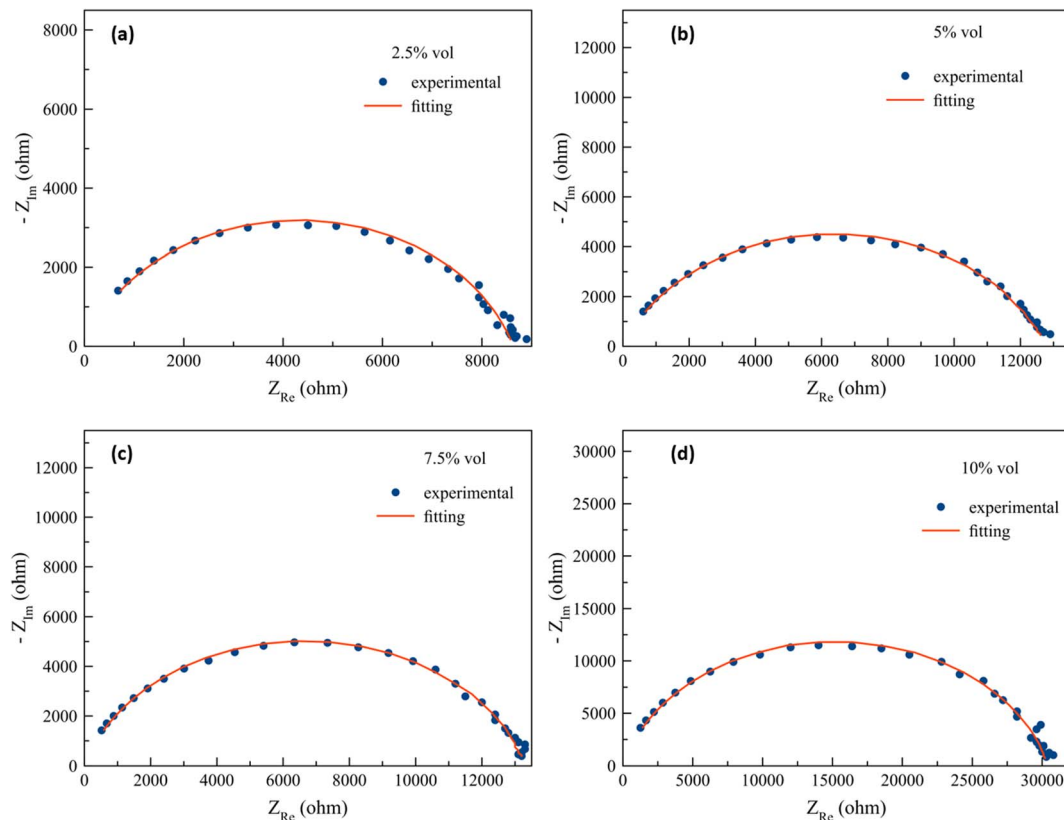
Fig. 6 The fitting results of the impedance curves of the PANI/m-ZrO$_2$ complex with: (a) 2.5% vol, (b) 5.0% vol, (c) 7.5% vol, and (d) 10% vol.

Table 5 Calculated parameters of Nyquist Plot

Sample	R (kΩ)	Q (Fs$^{\alpha-1}$)	α	GoF
PANI	8.17	1.14×10^{-8}	0.83	7.11×10^{-5}
PANI/a-ZrO$_2$	9.87	1.15×10^{-8}	0.81	5.50×10^{-5}
PANI/t-ZrO$_2$	9.16	4.42×10^{-9}	0.83	5.29×10^{-5}
PANI/m-ZrO$_2$ (2.5%)	8.63	1.19×10^{-8}	0.81	2.75×10^{-4}
PANI/m-ZrO$_2$ (5.0%)	12.76	1.81×10^{-8}	0.78	3.66×10^{-4}
PANI/m-ZrO$_2$ (7.5%)	13.31	1.07×10^{-8}	0.82	2.05×10^{-4}
PANI/m-ZrO$_2$ (10%)	30.41	3.24×10^{-9}	0.84	2.92×10^{-4}
PANI/tm-ZrO$_2$	79.59	9.34×10^{-9}	0.76	1.13×10^{-3}

presence of ZrO$_2$ filler decreased the dielectric losses. On the contrary, the higher the ZrO$_2$ filler contents in a material, the lower the dielectric losses. This phenomenon occurs because the dielectric constant and dielectric loss are more affected by the amorphous phase in the system.[32] From Fig. 8, the composite with amorphous ZrO$_2$ filler has lower dielectric loss than the composite with tetragonal zirconia filler. Fig. 7 and 8 show that the dielectric loss is more significant than the dielectric constant. Dielectric loss is affected by two things, namely, DC conductivity and dielectric polarization.[32] It can be seen in Table 5 that the DC conductivity of PANI/tm-ZrO$_2$ is the lowest, corresponding to the dielectric loss, which is also the lowest compared to the other samples.
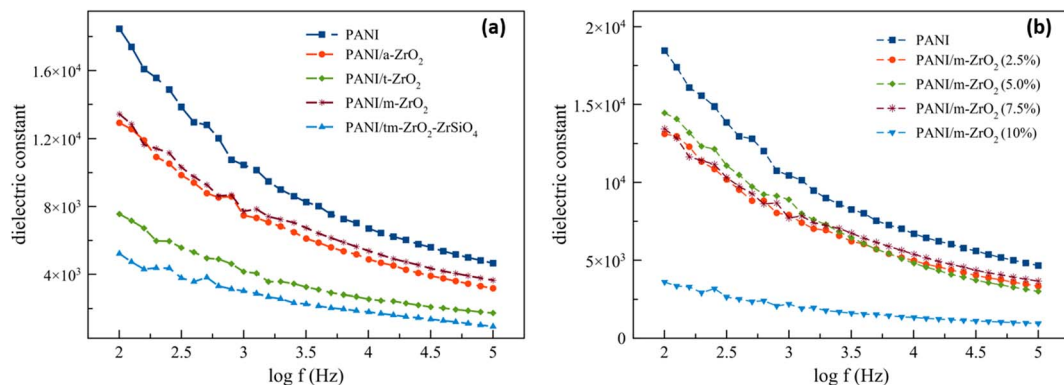

Fig. 7 Dielectric constants based on: (a) varied phases, (b) filler volume percentage.
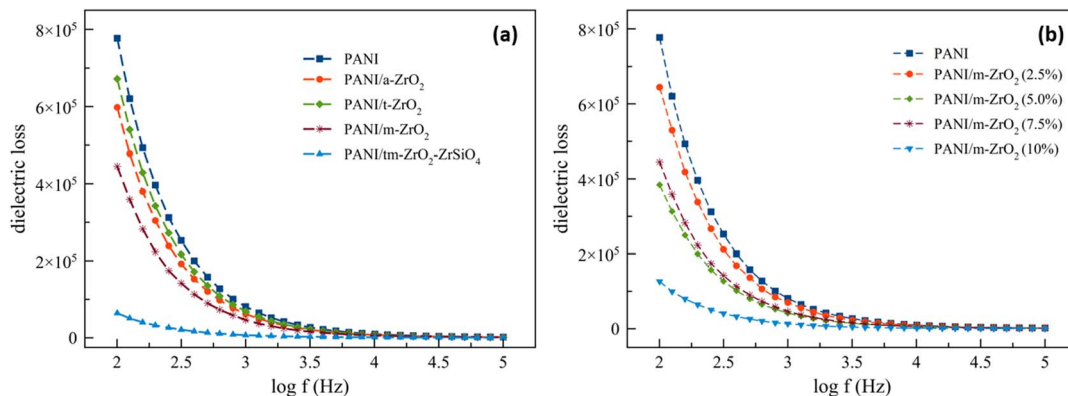
Fig. 8 Dielectric loss based on: (a) varied phases, (b) filler volume percentage.

3.4.3 Conductivity. The DC conductivity is calculated from eqn (5) as follows.

$$\sigma_{dc} = \left(\frac{1}{R}\right)\left(\frac{d}{A}\right) \quad (5)$$

Where R denotes the resistance values obtained from the fitting results of the Nyquist curve.

The AC conductivity however, is calculated from eqn (6) as follows.

$$\sigma_{ac} = \omega\varepsilon_0\varepsilon'' \quad (6)$$

The AC conductivity as a function of frequency is presented in Fig. 9. From Fig. 9, it is seen that the presence of ZrO$_2$ decreased the PANI conductivity. The comparison between the DC conductivity and AC conductivity at low frequencies are listed in Table 6.

The decrease in conductivity was possibly due to the presence of ZrO$_2$ particles considering that ZrO$_2$ is a ceramic material with insulator being one of their properties. At low frequencies, the conductivities decreased sequentially, starting from amorphous zirconia filler to tetragonal zirconia, monoclinic and zirconia fillers. There are materials with frequencies obtained at above 40 kHz, which are the tetragonal zirconia

Table 6 DC conductivity in comparison with AC conductivity at low frequency

Sample	σ_{dc} (S m^{-1})	σ_{ac} in low f (S m^{-1})
PANI	4.35×10^{-3}	4.34×10^{-3}
PANI/a-ZrO$_2$	3.33×10^{-3}	3.34×10^{-3}
PANI/t-ZrO$_2$	3.77×10^{-3}	3.75×10^{-3}
PANI/m-ZrO$_2$ (2.5%)	3.71×10^{-3}	3.60×10^{-3}
PANI/m-ZrO$_2$ (5.0%)	2.17×10^{-3}	2.14×10^{-3}
PANI/m-ZrO$_2$ (7.5%)	2.46×10^{-3}	2.48×10^{-3}
PANI/m-ZrO$_2$ (10%)	7.05×10^{-4}	7.06×10^{-4}
PANI/tm-ZrO$_2$	3.35×10^{-4}	3.58×10^{-4}

filler that has a conductivity below the composite with amorphous zirconia and monoclinic fillers. However, materials with tetragonal zirconia filler still have a higher conductivity when compared to composites with zirconia/zircon filler. The decrease in conductivity is due to the ceramic filler particles entering into the polymers, which is possibly caused by the presence of metal oxide particles that reduced the interconnections between the polymer chains, which in turned reduced the electrical transports.[39]

The results above show that the PANI/ZrO$_2$ composite has electrical conductivity in the semiconductor range, a high
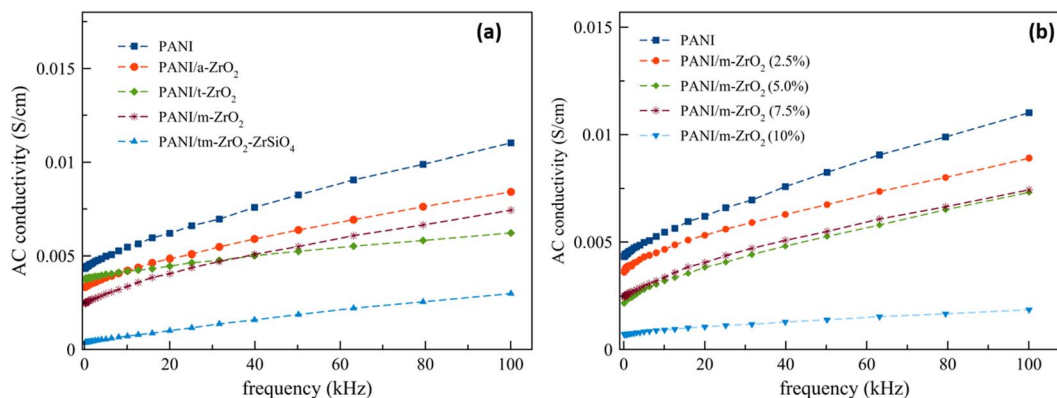

Fig. 9 AC conductivity based on: (a) varied phases, (b) filler volume percentage.

dielectric constant, and the potential for application as an anticorrosive material. It is generally believed that conductive polymer coatings can protect metals by forming a physical barrier, inhibition and passive oxide layer.[40] In addition, the PANI/ZrO$_2$ composite has been known to have good thermal stability.[41] Combining these two properties allows for applications such as corrosion protection at high temperatures.

4. Conclusions

PANI and PANI/ZrO$_2$ composite polymorphisms have been successfully synthesized using the *in situ* polymerization method. The composite structures have been confirmed *via* the data obtained from XRD and FTIR. The morphology of PANI and PANI/ZrO$_2$ polymorphisms were verified to be in the shape of semi-tubular. ZrO$_2$ polymorphism as a filler affected the electrical properties of PANI/ZrO$_2$ composite. The impedance of PANI/ZrO$_2$ was found to be larger than PANI, where the largest impendance was produced by the multiphase filler (ZrO$_2$–ZrSiO$_4$). PANI and PANI/ZrO$_2$ both have a high dielectric constants, thus both can be categorised as a material with a high permittivity (high-k). Despite being so, their dielectric constants and dielectric losses of PANI/ZrO$_2$ were also found to be lower than PANI. The AC electricity conductivity of PANI/ZrO$_2$ was also found lower compared to PANI.

Besides from the phase, the filler composition also affected the electrical properties of PANI/ZrO$_2$. The higher the filler percentage resulted in an increase in the impedance. The highest impedance obtained was at 10% volume of ZrO$_2$. The increase in filler composition contributed to the decrease in dielectric constant and dielectric losses as well as the electrical conductivity when compared to PANI. PANI/ZrO$_2$ composites have potential applications for corrosion protection at high temperatures.

Author contributions

Munaji: investigation, data curation, formal analysis, methodology, visualization, original writing draft. Mochamad Zainuri: conceptualization, supervision, methodology. Triwikantoro: conceptualization, supervision, writing – review & editing.

Conflicts of interest

There are no conflicts to declare.

Acknowledgements

References

1 P. Sengupta, A. Bhattacharjee and H. S. Maiti, Zirconia: A Unique Multifunctional Ceramic Material, *Trans. Indian Inst. Met.*, 2019, **72**, 1981–1998.

2 M. Musyarofah, *et al.*, Synthesis of high-purity zircon, zirconia, and silica nanopowders from local zircon sand, *Ceram. Int.*, 2019, **45**, 6639–6647.

3 C. F. K. Murti, U. Maslakah, E. Endarko and T. Triwikantoro, Structural, physical and mechanical properties of zirconia-polymorph/alumina composites, *Mater. Chem. Phys.*, 2022, **285**, 126102.

4 R. Romero Pareja, R. López Ibáñez, F. Martín, J. R. Ramos-Barrado and D. Leinen, Corrosion behaviour of zirconia barrier coatings on galvanized steel, *Surf. Coat. Technol.*, 2006, **200**, 6606–6610.

5 J. H. Sui and W. Cai, Formation of ZrO$_2$ coating on the NiTi alloys for improving their surface properties, *Nucl. Instrum. Methods Phys. Res., Sect. B*, 2006, **251**, 402–406.

6 M. Menkuer and H. Ozkazanc, Anticorrosive polypyrrole/zirconium-oxide composite film prepared in oxalic acid and dodecylbenzene sulfonic acid mix electrolyte, *Prog. Org. Coat.*, 2020, **147**, 105815.

7 S. V. Harb, *et al.*, A comparative study on PMMA-TiO$_2$ and PMMA-ZrO$_2$ protective coatings, *Prog. Org. Coat.*, 2020, **140**, 105477.

8 M. A. Reyes-Acosta, *et al.*, Influence of ZrO$_2$ nanoparticles and thermal treatment on the properties of PMMA/ZrO$_2$ hybrid coatings, *J. Alloys Compd.*, 2015, **643**, S150–S158.

9 S. Devikala, P. Kamaraj and M. Arthanareeswari, Corrosion resistance behavior of PVDF/ZrO$_2$ composite in 3.5% NaCl, *Mater. Today: Proc.*, 2019, **14**, 279–287.

10 G. K. Sidhu, N. Kumar & R. Kumar Study the structural and optical behaviour of polyaniline/ZrO$_2$ nanocomposites, in *AIP Conference Proceedings*, American Institute of Physics Inc., 2018, vol. 1953.

11 T. Anwer, M. O. Ansari and F. Mohammad, Dodecylbenzenesulfonic acid micelles assisted in situ preparation and enhanced thermoelectric performance of semiconducting polyaniline-zirconium oxide nanocomposites, *J. Ind. Eng. Chem.*, 2013, **19**, 1653–1658.

12 B. P. Prasanna, *et al.*, Synthesis of polyaniline/ZrO$_2$ nanocomposites and their performance in AC conductivity and electrochemical supercapacitance, *Bull. Mater. Sci.*, 2016, **39**, 667–675.

13 D. Zhao, X. Liu, Z. Li and X. Bai, Effect of emulsion polymerisation conditions on electrical performance of polyaniline, *Pigm. Resin Technol.*, 2011, **40**, 84–90.

14 Y. Kriswandono, M. Munaji and T. Triwikantoro, Electrical Conductivity of SDBS-Assisted Polyaniline Doped with HCl, *Mater. Sci. Forum*, 2022, **1057**, 26–31.

15 L. Shao, J. W. Jeon and J. L. Lutkenhaus, Polyaniline nanofiber/vanadium pentoxide sprayed layer-by-layer electrodes for energy storage, *J. Mater. Chem. A*, 2014, **2**, 14421–14428.

16 M. H. Bai, T. Y. Liu, F. Luan, Y. Li and X. X. Liu, Electrodeposition of vanadium oxide-polyaniline composite nanowire electrodes for high energy density supercapacitors, *J. Mater. Chem. A*, 2014, **2**, 10882–10888.

17 S. Bai, Y. Ma, R. Luo, A. Chen and D. Li, Room temperature triethylamine sensing properties of polyaniline-WO3 nanocomposites with p–n heterojunctions, *RSC Adv.*, 2016, **6**, 2687–2694.

18 D. Hidalgo, S. Bocchini, M. Fontana, G. Saracco and S. Hernández, Green and low-cost synthesis of PANI-TiO$_2$ nanocomposite mesoporous films for photoelectrochemical water splitting, *RSC Adv.*, 2015, **5**, 49429–49438.

19 N. Singh, *et al.*, Development of a potential LPG sensor based on a PANI-Co$_3$O$_4$ nanocomposite that functions at room temperature, *New J. Chem.*, 2019, **43**, 17340–17350.

20 Z. Durmus, A. Baykal, H. Kavas and H. Szeri, Preparation and characterization of polyaniline (PANI)Mn$_3$O$_4$ nanocomposite, *Phys. B*, 2011, **406**, 1114–1120.

21 B. N. Grgur, *et al.*, Corrosion of mild steel with composite polyaniline coatings using different formulations, *Prog. Org. Coat.*, 2015, **79**, 17–24.

22 S. Shi, Z. Zhang and L. Yu, Hydrophobic polyaniline/ modified SiO$_2$ coatings for anticorrosion protection, *Synth. Met.*, 2017, **233**, 94–100.

23 W. F. Huang, *et al.*, Super-hydrophobic polyaniline-TiO$_2$ hierarchical nanocomposite as anticorrosion coating, *Mater. Lett.*, 2020, **258**, 126822.

24 F. C. P. Masim, *et al.*, Synergistic effect of PANI–ZrO$_2$ composite as antibacterial, anti-corrosion, and phosphate adsorbent material: synthesis, characterization and applications, *Environ. Technol.*, 2019, **40**, 226–238.

25 M. V. Carević, *et al.*, Properties of Zirconia/Polyaniline hybrid nanocomposites and their application as photocatalysts for degradation of model pollutants, *Mater. Chem. Phys.*, 2018, **205**, 130–137.

26 T. Anwer, M. O. Ansari and F. Mohammad, Morphology and Thermal Stability of Electrically Conducting Nanocomposites Prepared by Sulfosalicylic Acid Micelles Assisted Polymerization of Aniline in Presence of ZrO$_2$ Nanoparticles, *Polym.-Plast. Technol. Eng.*, 2013, **52**, 472–477.

27 H. Huang, Z. C. Guo, W. Zhu and F. C. Li, Preparation and characterization of conductive polyaniline/zirconia nanoparticles composites, *Adv. Mater. Res.*, 2011, **221**, 302–307.

28 S. M. Rezaei Niya and M. Hoorfar, On a possible physical origin of the constant phase element, *Electrochim. Acta*, 2016, **188**, 98–102.

29 R. Srinivasan & F. Fasmin, *An Introduction to Electrochemical Impedance Spectroscopy*, CRC Press, 2021.

30 Z. Kerner and T. Pajkossy, On the origin of capacitance dispersion of rough electrodes, *Electrochim. Acta*, 2000, **46**, 207–211.

31 B. Hirschorn, *et al.*, Determination of effective capacitance and film thickness from constant-phase-element parameters, *Electrochim. Acta*, 2010, **55**, 6218–6227.

32 M. B. Ahmed, *et al.*, The study of ion transport parameters associated with dissociated cation using EIS model in solid polymer electrolytes (SPEs) based on PVA host polymer: XRD, FTIR, and dielectric properties, *Arabian J. Chem.*, 2022, **15**, 104196.

33 N. Nadliriyah, A. L. Putri & T. Triwikantoro PANi/ZrO$_2$-composite coating for corrosion protection in 3.5 M NaCl solution. in *IOP Conference Series: Materials Science and Engineering*, Institute of Physics Publishing, 2019, vol. 496.

34 M. Guo, *et al.*, Preparation of Nano-ZrO$_2$ powder via a microwave-assisted hydrothermal method, *Ceram. Int.*, 2021, **47**, 12425–12432.

35 T. Velempini, E. Prabakaran and K. Pillay, Photocatalytic reductive applications of C-doped ZrO$_2$/PANI composite towards Cr(VI), *J. Photochem. Photobiol., A*, 2022, **426**, 113737.

36 Z. M. Dang, *et al.*, Fundamentals, processes and applications of high-permittivity polymer-matrix composites, *Prog. Mater. Sci.*, 2012, **57**, 660–723.

37 S. Jiang, L. Jin, H. Hou & L. Zhang Polymer-based nanocomposites with high dielectric permittivity, *Polymer-Based Multifunctional Nanocomposites and Their Applications*, Elsevier Inc., 2018, DOI: 10.1016/B978-0-12-815067-2.00008-1.

38 R. Patil, A. S. Roy, K. R. Anilkumar, K. M. Jadhav and S. Ekhelikar, Dielectric relaxation and ac conductivity of polyaniline-zinc ferrite composite, *Composites, Part B*, 2012, **43**, 3406–3411.

39 I. Bekri-Abbes and E. Srasra, Characterization and AC conductivity of polyaniline-montmorillonite nanocomposites synthesized by mechanical/chemical reaction, *React. Funct. Polym.*, 2010, **70**, 11–18.

40 H. Xu and Y. Zhang, A review on conducting polymers and nanopolymer composite coatings for steel corrosion protection, *Coatings*, 2019, **9**, 1–22.

41 S. Wang, Z. Tan, Y. Li, L. Sun and T. Zhang, Synthesis, characterization and thermal analysis of polyaniline/ZrO 2 composites, *Thermochim. Acta*, 2006, **441**, 191–194.